

Supporting Information

Achieving High Gravimetric Energy Density for Flexible Lithium Ion Batteries Facilitated by Core-Double-Shell Electrodes

**Muhammad-Sadeeq Balogun^{†1}, Hao Yang^{†1}, Yang Luo¹, Weitao Qiu¹,
Yongchao Huang², Zhao-Qing Liu^{*2} and Yexiang Tong^{*1}**

¹MOE Laboratory of Bioinorganic and Synthetic Chemistry/The Key Lab of Low-Carbon Chemistry and Energy Conservation of Guangdong Province/School of Chemistry, Sun Yat-sen University, 135, Xingang West Road, Guangzhou, 510275, China

²School of Chemistry and Chemical Engineering/Key Laboratory for Water Quality and Conservation of the Pearl River Delta, Ministry of Education/Research Institute of Environmental Studies at Greater Bay, Guangzhou University, Guangzhou Higher Education Mega Center, Outer Ring Road No. 230, Guangzhou 510006, China Corresponding Authors E-mail: lzqgz@gzhu.edu.cn; chedhx@mail.sysu.edu.cn

[†]These authors contribute equally to this work.

Calculations

Energy and Power Density Calculations

$$\text{Energy density (Wh kg}^{-1}\text{)}, E = C_{\text{cell}} \times \Delta V \quad (1)$$

where C_{cell} is the discharge capacity of the cell and V is the testing voltage windows.

$$\text{Power density (W kg}^{-1}\text{)}, P = E/1000 \times \Delta t \quad (2)$$

where E is the energy density and t is the time required for discharging.

DFT Calculations

All the calculations were performed based on spin-polarized periodic density functional theory (DFT) implemented in Gaussian 09W.¹ The calculation basis set was B3LYP and the total energy convergence was set to be lower than 10^{-5} eV, and the force convergence was set to be smaller than 0.02 eV/Å. The potential of all the calculations were set to 0 V.

The Gibbs free energy change (ΔG) of each reaction step is calculated as:

$$\Delta G = E_{\text{tot(b)}} - E_{\text{tot(a)}} + \Delta E_{\text{ZPE}} - T\Delta S$$

where $E_{\text{tot(b)}}$ is the energy of the given unit cell with intermediate of the latter state, $E_{\text{tot(a)}}$ is the energy of the intermediate of the previous state, ΔE_{ZPE} is the difference corresponding to the zero point energy change between the intermediates of the previous state and the latter state, ΔS is entropy change between the intermediates of the previous state and the latter state, T represents the temperature applied for lithium storage performance.

Supplementary Figures

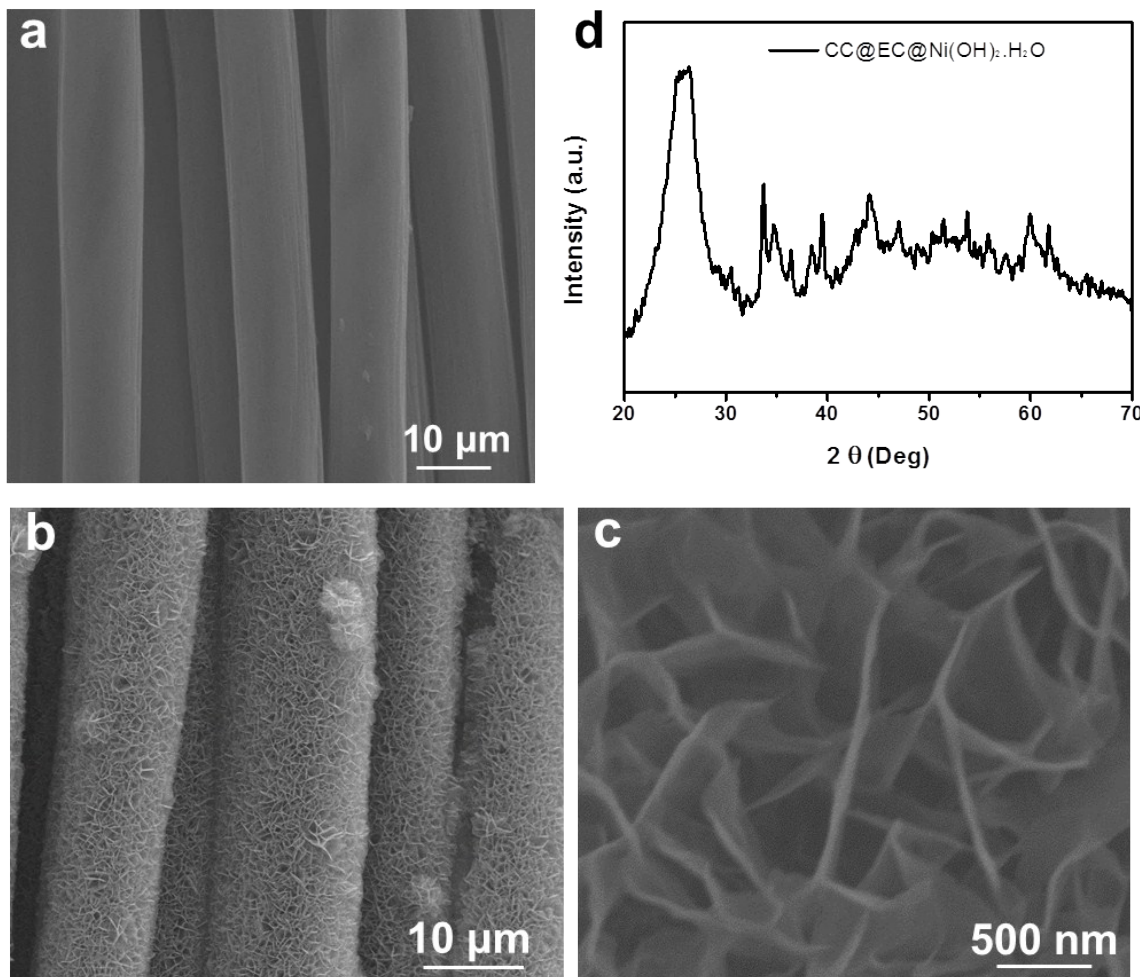


Figure S1. SEM images of (a) pristine CC and (b) CC@Ni(OH)·H₂O. (c) Magnified SEM image of CC@Ni(OH)·H₂O. (d) XRD spectra of CC@Ni(OH)·H₂O.

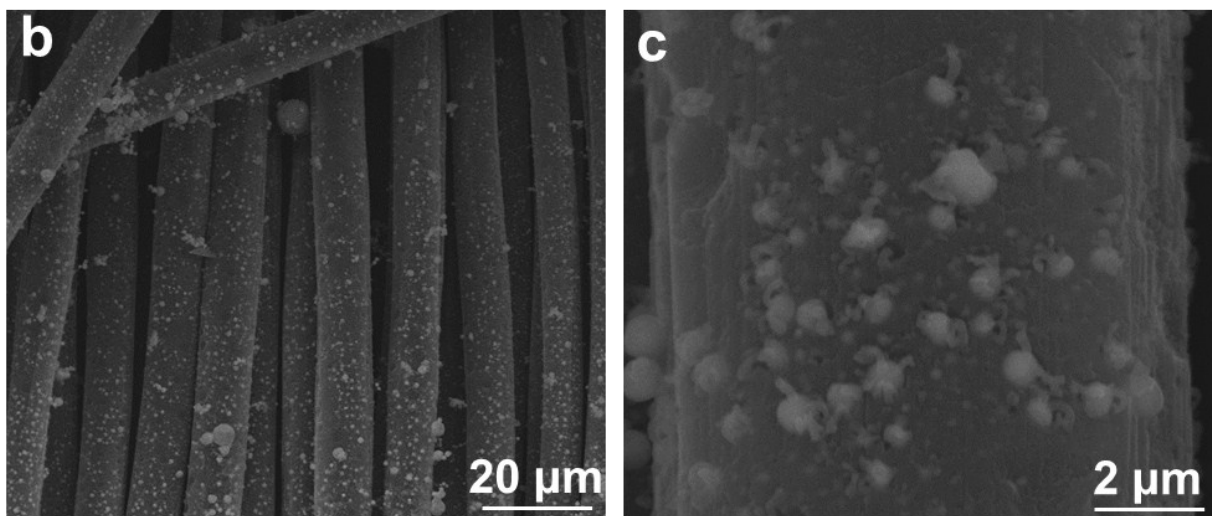
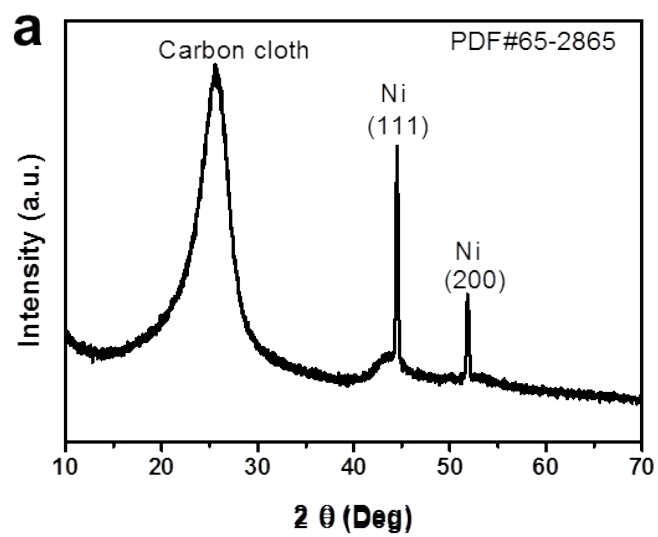


Figure S2. (a) XRD spectra of CC@Ni. (b and c) SEM images of CC@Ni.

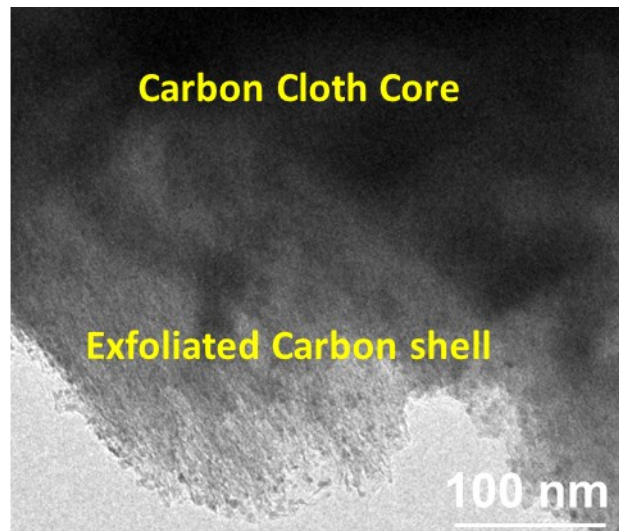


Figure S3. TEM image of CC@EC showing the CC core and EC shell.

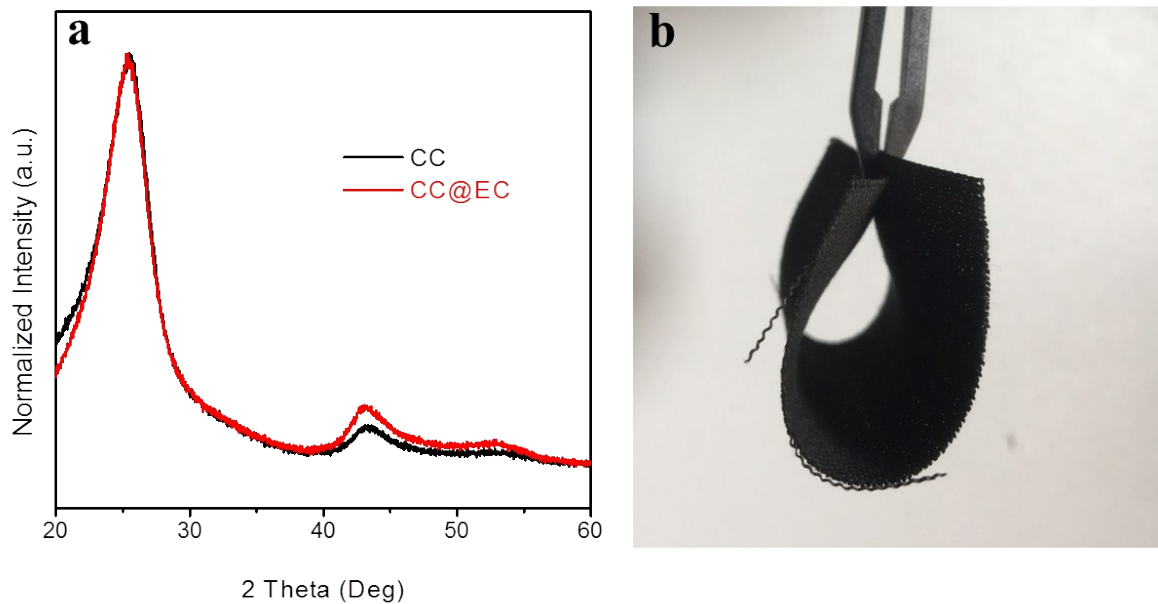


Figure S4. (a) XRD spectra of CC and CC@EC substrate. (b) digital image of CC@EC showing its flexibility.

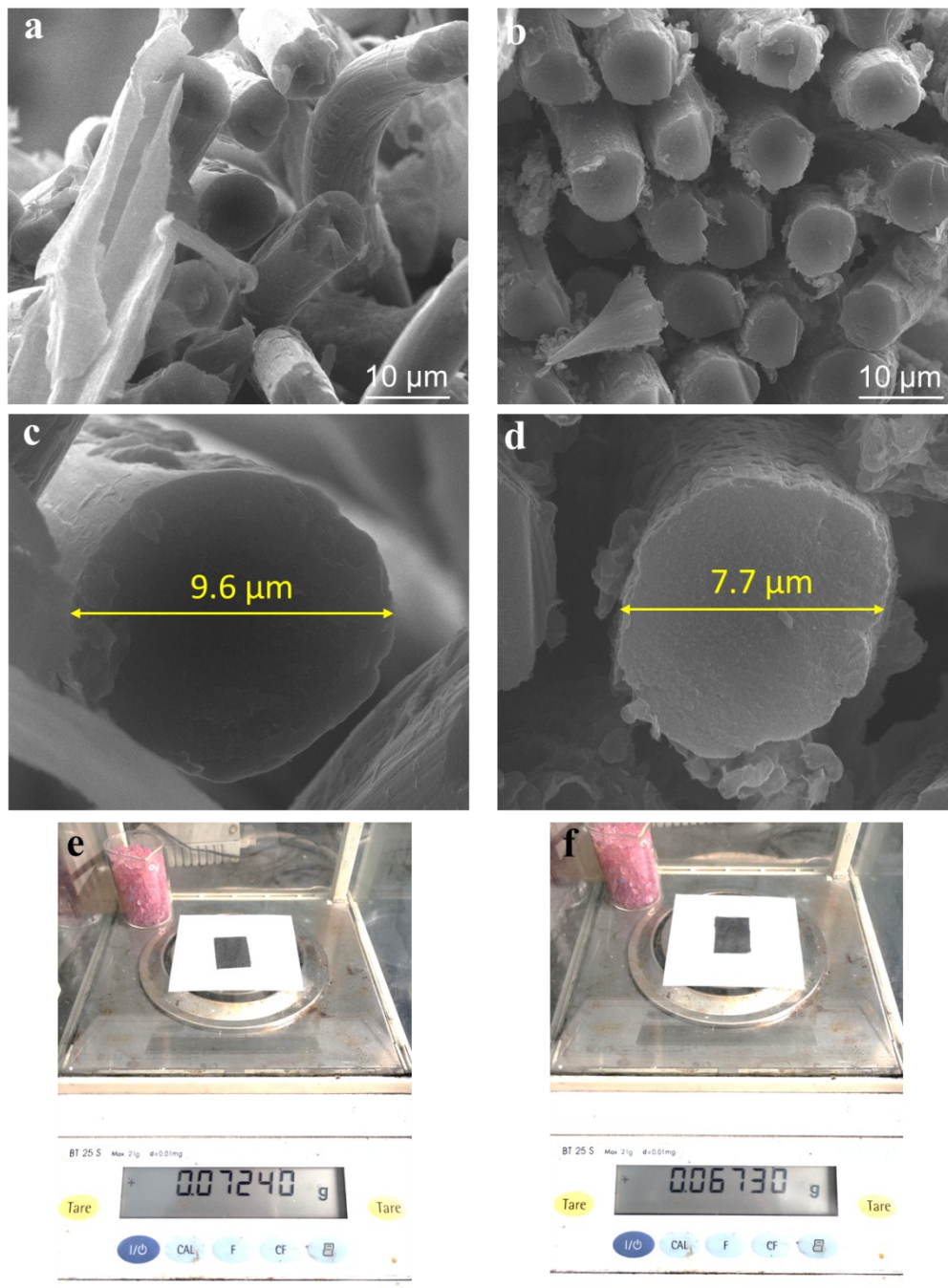


Figure S5. Low magnification SEM images showing the side view of the (a) CC and (b) CC@EC. Magnified SEM images showing the thickness of the (c) CC and (d) CC@EC. Mass of (e) CC before post-treatment reactions and (f) CC@EC.

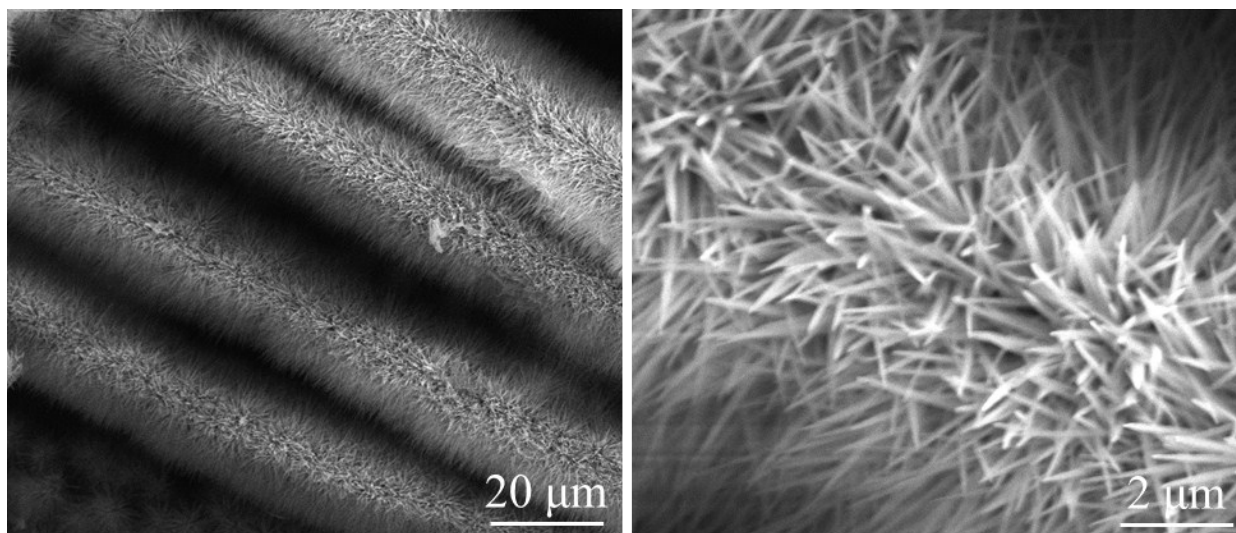


Figure S6. SEM images showing of NiCo nanowires precursor grown on CC@EC.

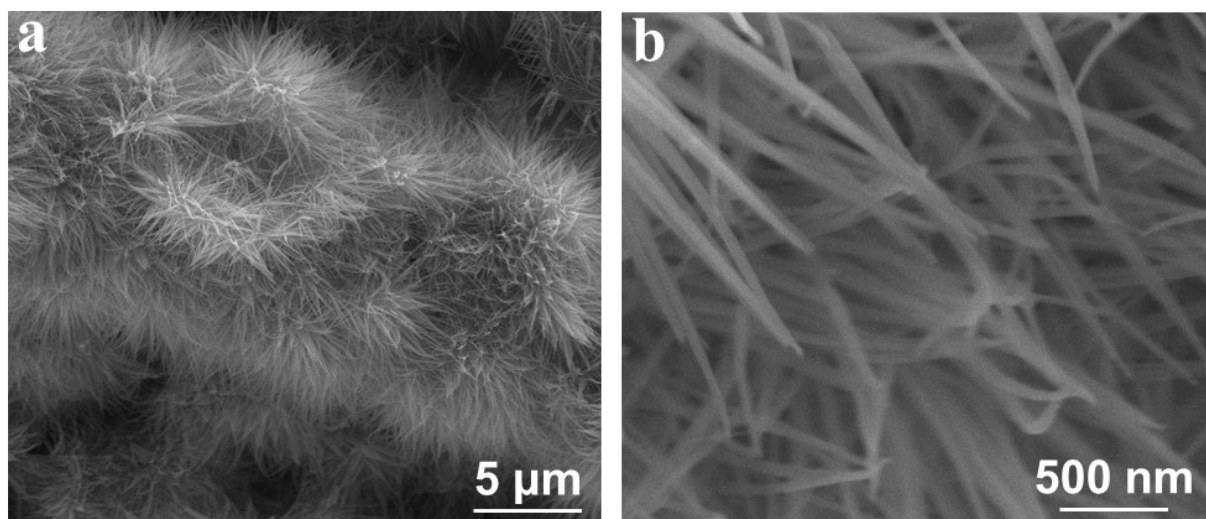


Figure S7. SEM images showing of CC@NCO.

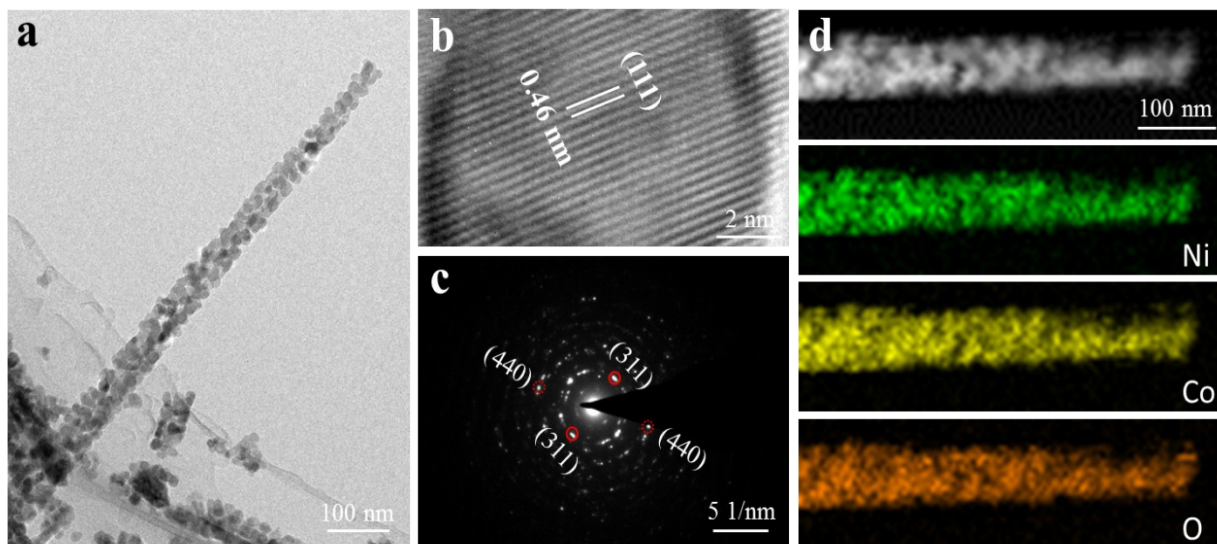


Figure S8. TEM characterization and EDX elemental mapping of NCO nanowire.

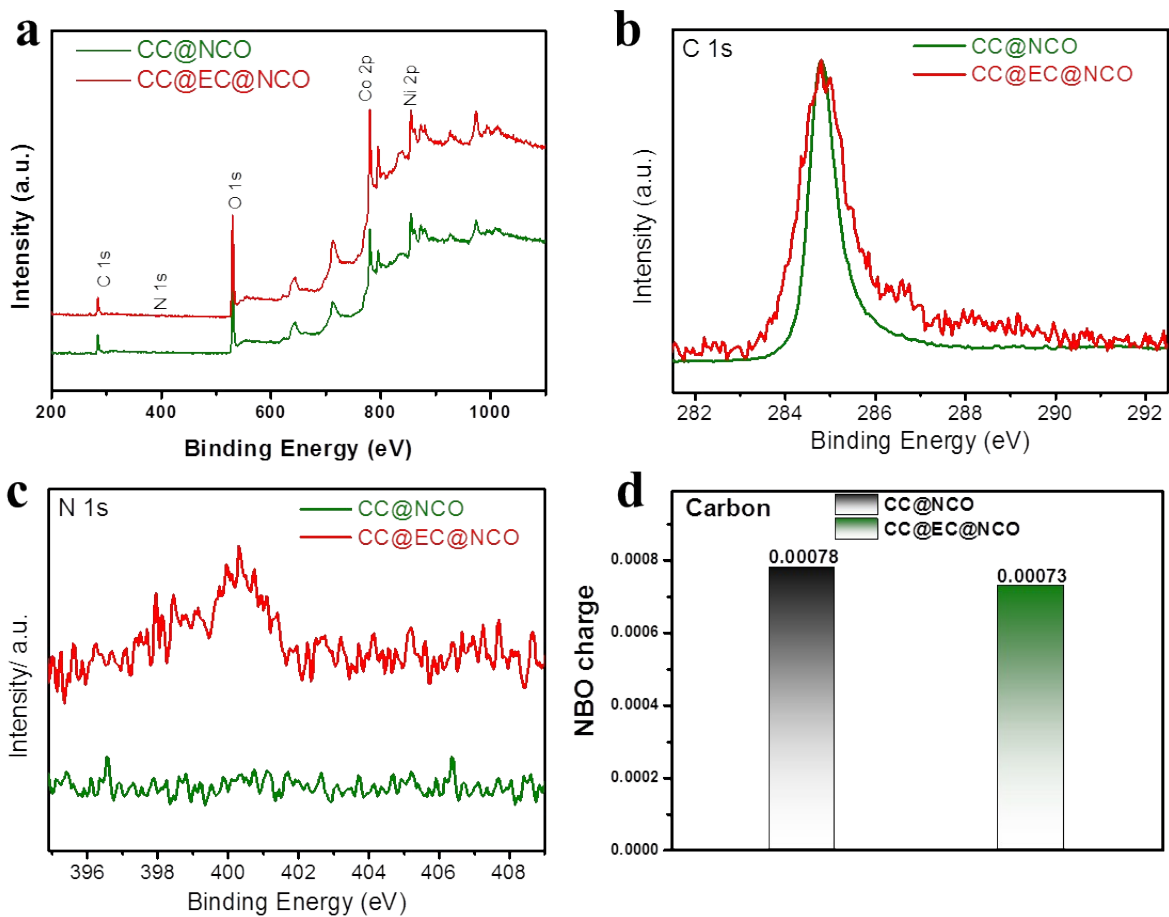


Figure S9. (a) XPS survey spectra of CC@NCO and CC@EC@NCO. Gauss (b) C 1s and (c) N 1s XPS spectra of CC@NCO and CC@EC@NCO. (d) Charge density distributions of C on CC@NCO and CC@EC@NCO.

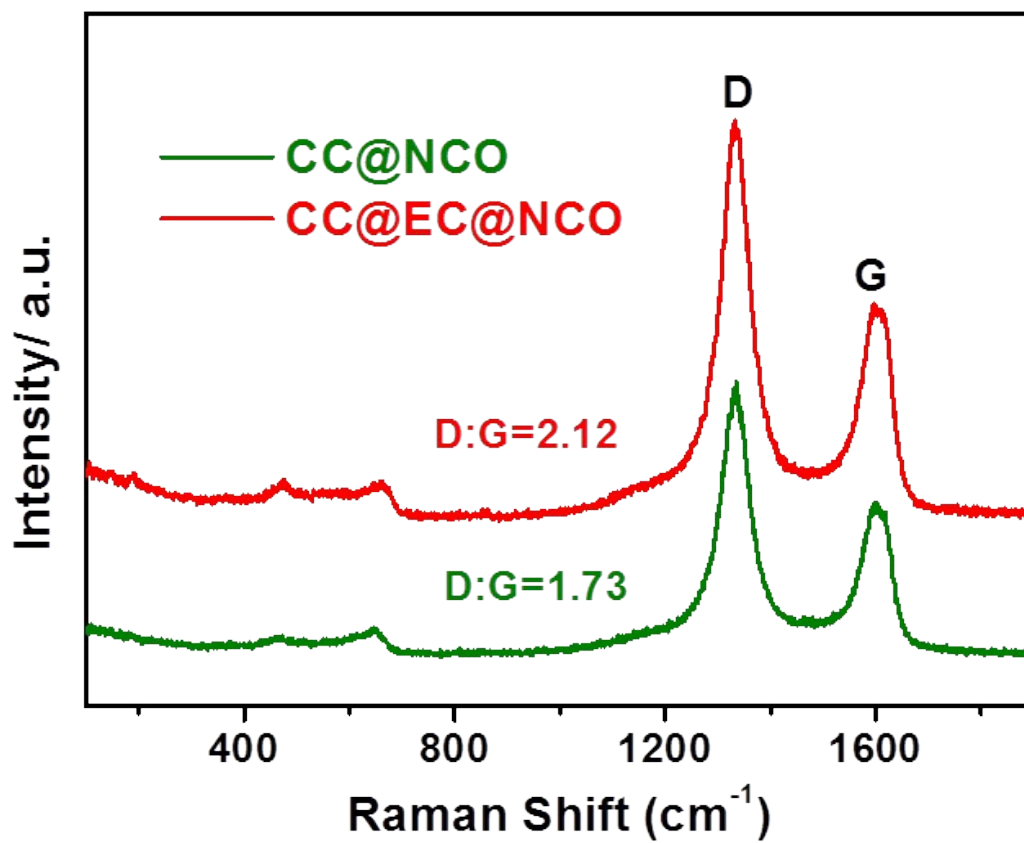


Figure S10. (a) Raman spectra of CC@NCO and CC@EC@NCO showing the D:G.

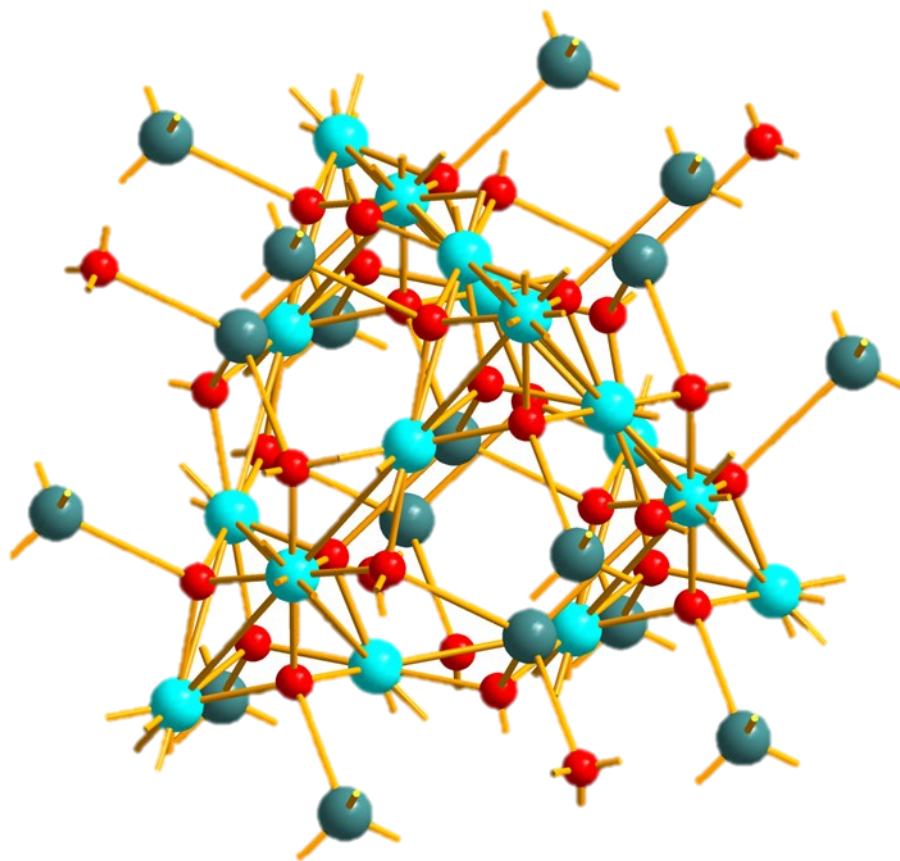


Figure S11. Simplified and optimized NCO cluster for DFT calculations.

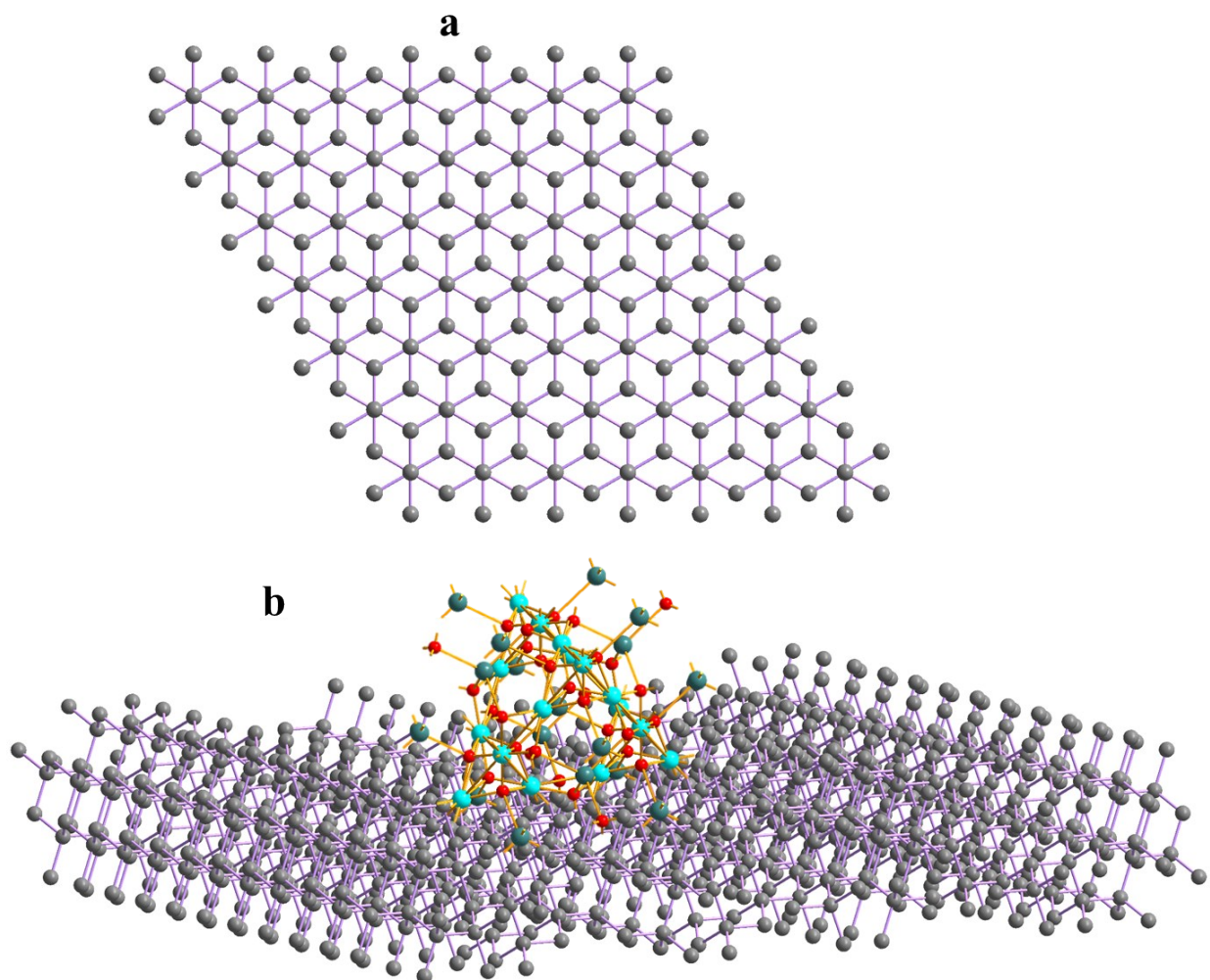


Figure S12. Simplified and optimized (a) CC and (b) CC@NCO clusters for DFT calculations.

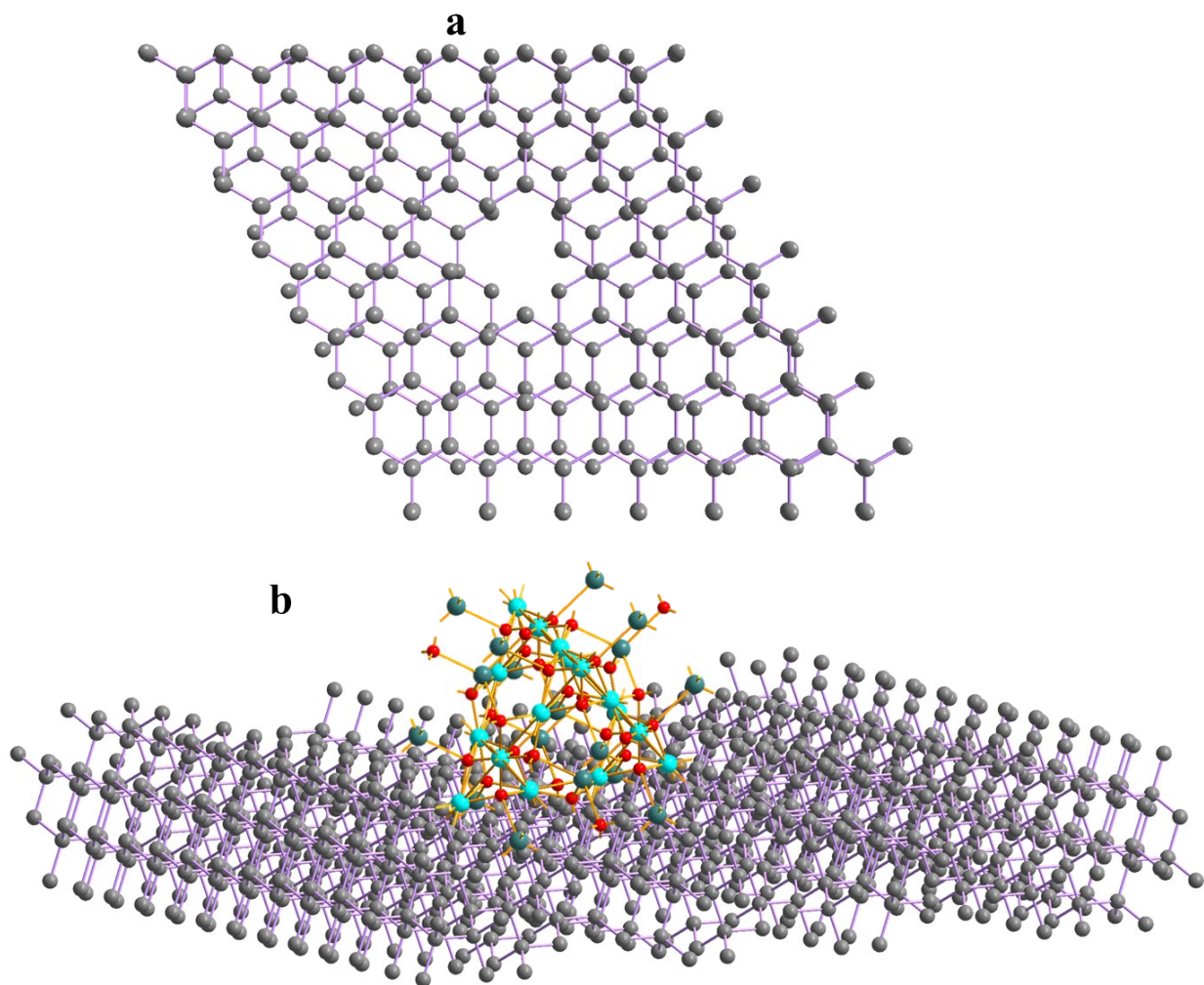


Figure S13. Simplified and optimized (a) CC@EC and (b) CC@EC@NCO clusters for DFT calculations.

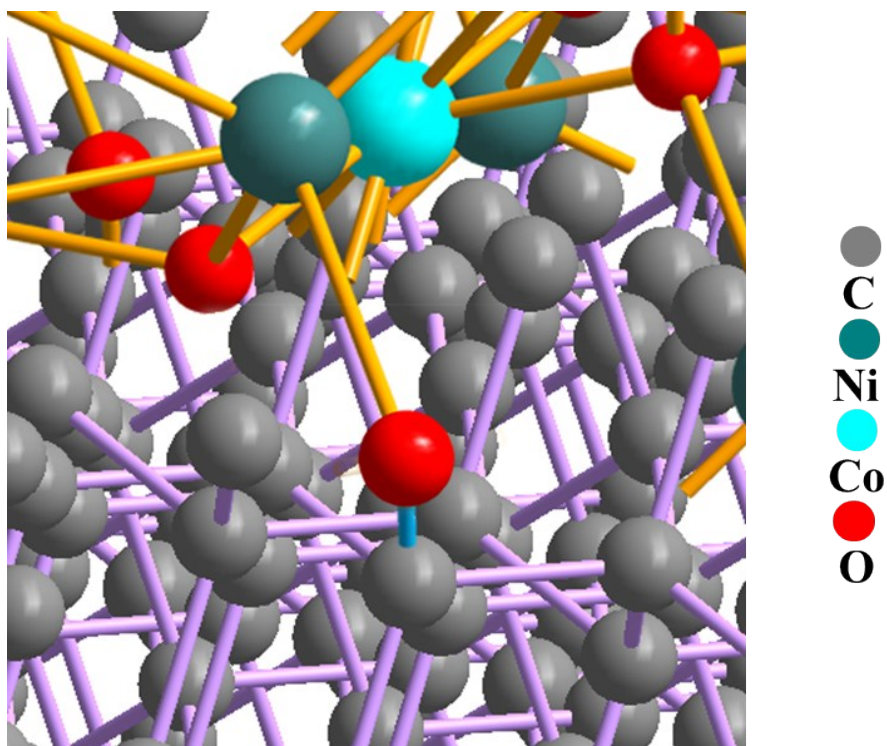


Figure S14. Enlarged snapshot of covalent bonds between O (functional group of ECC) and Co (from NCO).

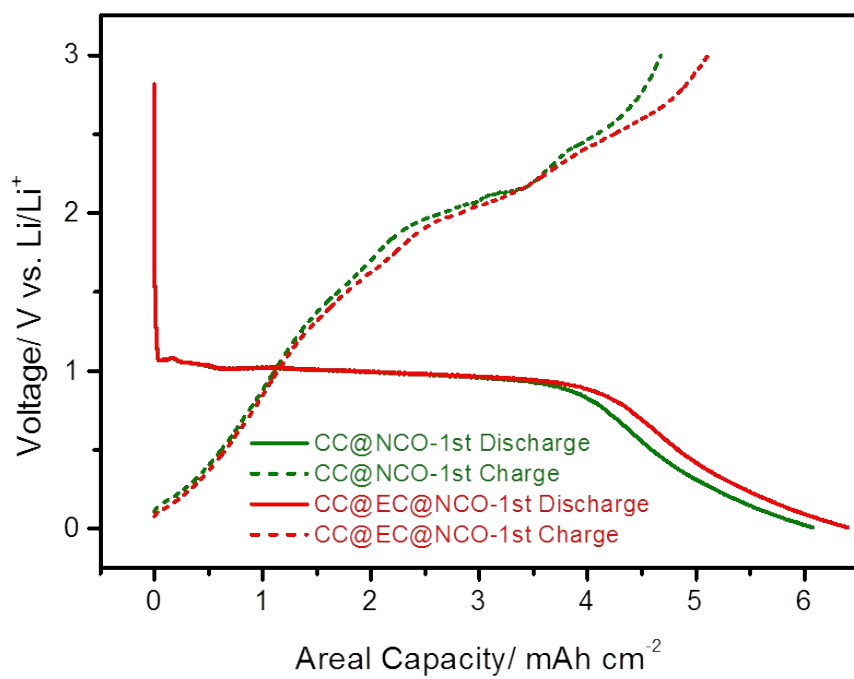


Figure S15. (a) 1st discharge-charge profile CC@EC@NCO and CC@NCO electrodes.

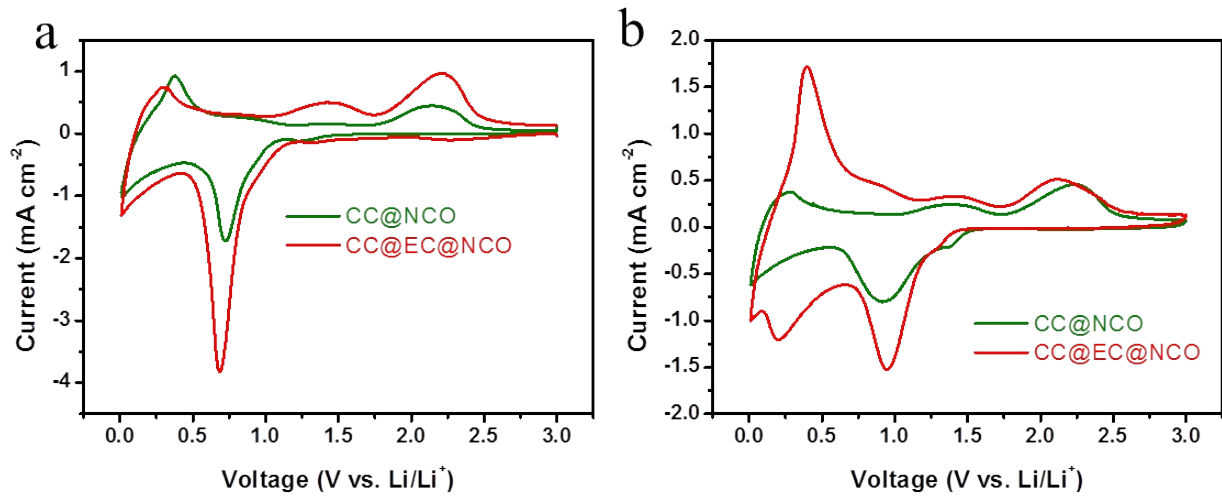


Figure S16. (a) 1st and (b) 3rd CV curves of CC@EC and (b) CC@EC@NCO electrodes.

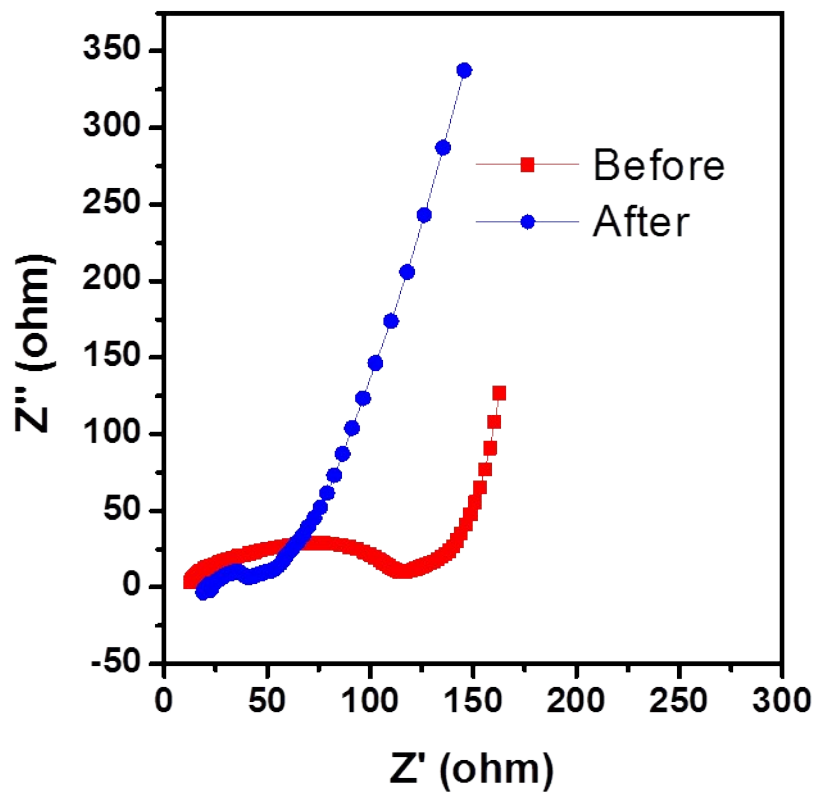


Figure S17. Nyquist plot of CC@EC@NCO electrode before and after rate performance.

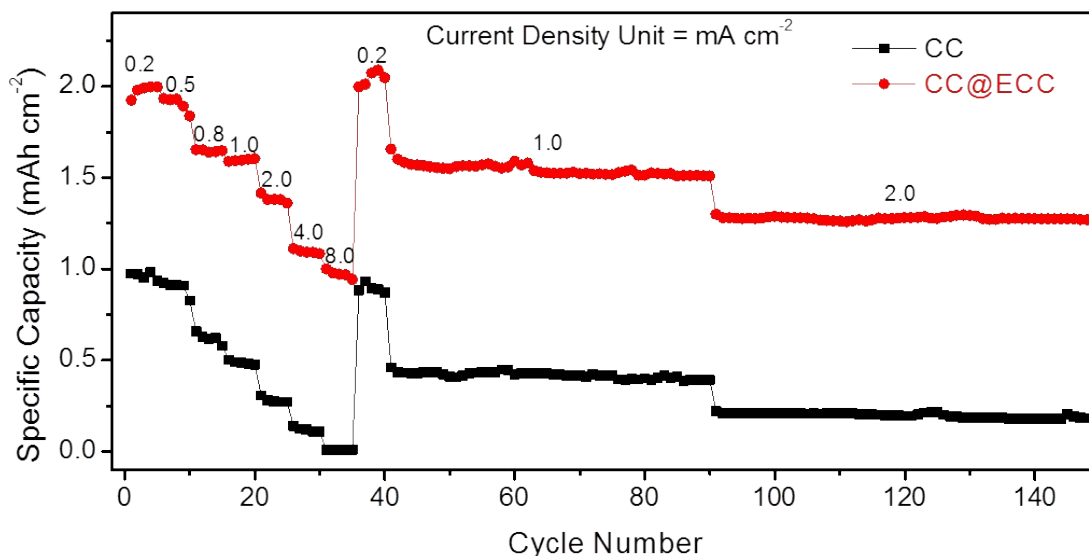


Figure S18. Lithium storage performance of CC and CC@EC anodes.

Capacity Contribution of the Carbon Cloth

Firstly, according to Figure 3d, the capacity contribution of the CC@EC to the CC@EC@NCO electrode during the 1st discharge cycle is 1.54 mAh cm⁻², while that of CC@NC is 1.32 mAh cm⁻². After the 2nd cycle, capacity contribution of 1.48 mAh cm⁻² was achieved by the CDS electrode and that of CC@NCO could only reach 1.07 mAh cm⁻² (Figure 3e).

The capacity contribution from the carbon cloth substrate is quite less compare to the total capacity of the electrode. We can calculate the capacity contribution of the carbon cloth based on the calculation below:

CC@EC@NCO

The total mass of the electrode (1.0 cm²) is around 14.5 mg (~4 mg NCO, 10.5 mg CC@EC). The electrode has a capacity of ~4.49 mAh cm⁻² at 0.3 mA cm⁻².

According to Figure S17, the capacity of 1.0 cm² CC@ECC electrode is 2.27 mAh cm⁻².

Therefore, the capacity percentage of the CC@EC: $2.27/4.49 = 51\%$.

The total capacity of based on the NCO anode is estimated: 1122.5 mAh g⁻¹.

Hence, the CC@EC contribution can be estimated: 51% of 1122.5 mAh g⁻¹ = 572.5 mAh g⁻¹

CC@NCO

The total mass of the electrode (1.0 cm²) is around 16.5 mg (~4 mg NCO, 12.5 mg CC).

The electrode has a capacity of ~2.59 mAh cm⁻² at 0.3 mA cm⁻².

According to Figure S17, the capacity of 1.0 cm² CC@ECC electrode is 0.93 mAh cm⁻².

Therefore, the capacity percentage of the carbon cloth: 0.93/2.59 = 36%.

The total capacity of based on the NCO anode is estimated: 647.5 mAh g⁻¹.

Hence, the CC contribution can be estimated: 36% of 647.5 mAh g⁻¹ = 233.1 mAh g⁻¹

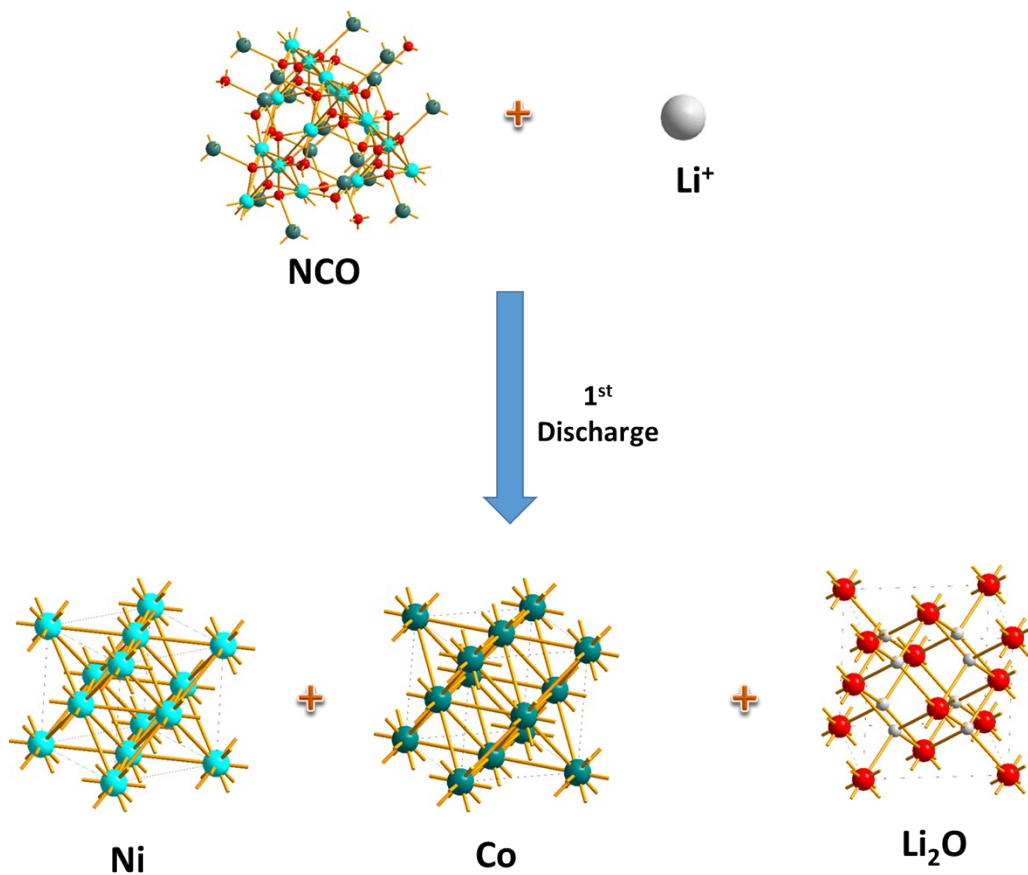


Figure S19. Simplified and optimized of NCO clusters during the first discharge cycle for DFT calculations.

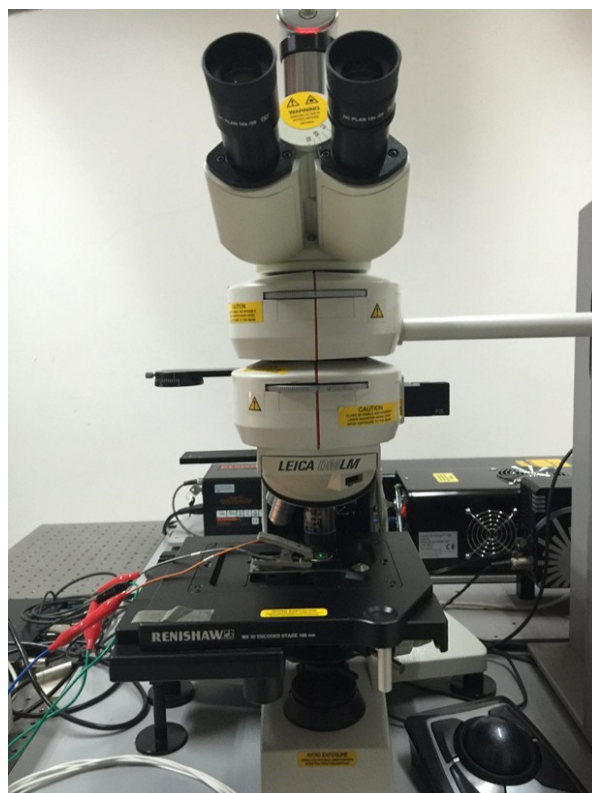


Figure S20. Digital image of the *in situ* Raman set-up.

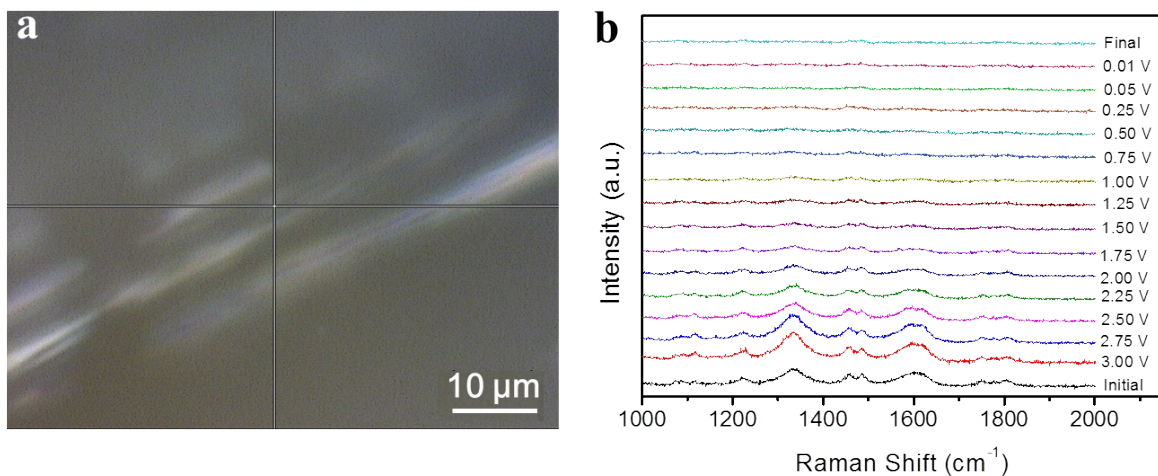


Figure S21. (a) SEM image of the point where Raman spectra were collected for CC@NCO cell. (b) *In situ* Raman spectra of CC@NCO at different intercalated voltages. (i) Plot of the I_D/I_G vs. intercalated voltages for CC@NCO.

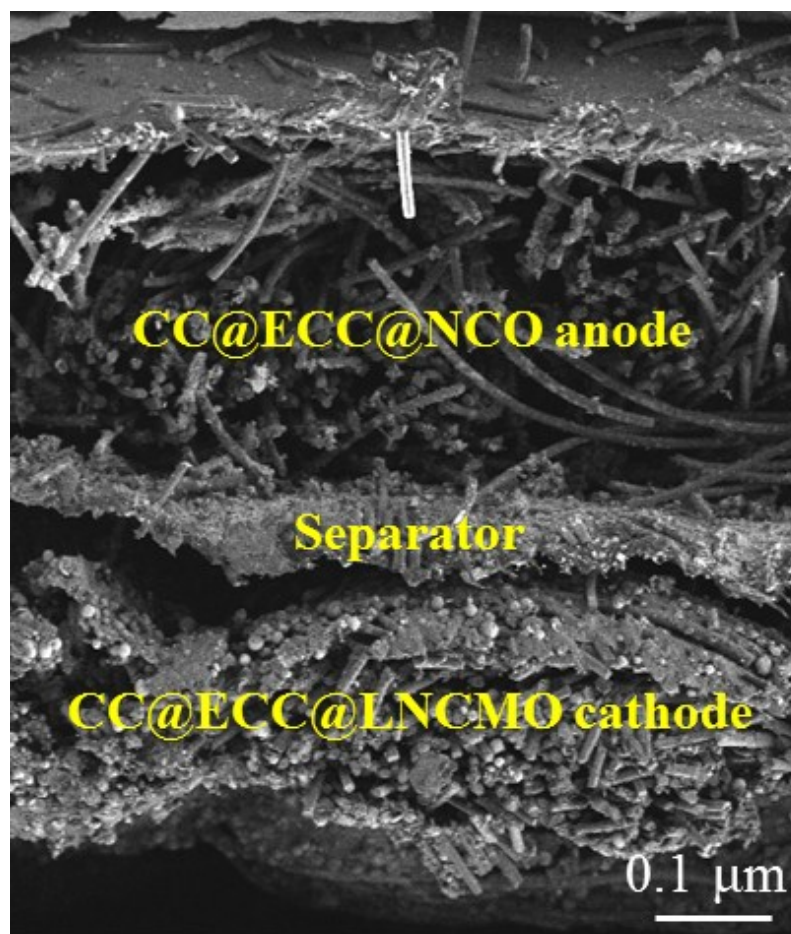


Figure S22. (a) Side-view SEM image of the CC@EC@NCO//CC@EC@LNCMO AFLIB.

Commercial LiNiCoMnO₂ (LNCMO) Cathode

For the cathode material, the electrode was fabricated by mixing the LNCMO powder and PVDF binder at weight ratios of 90:10. The slurry was then casted on the CC and CC@EC substrate, transferred to a vacuum oven and dried at 110 °C overnight. Half cells were also assembled in a coin cell using 1 M LiPF₆ in ethylene carbonate (EC) and diethyl carbonate (DEC) [(1:1)] solution as the electrolyte, Celgard 2400 was used as the separator and Li foil as both counter and reference electrodes. The galvanostatic charge/discharge tests were carried out between 2.0–4.5 V for cathode on a Neware Battery Testing System (Shenzhen, China).

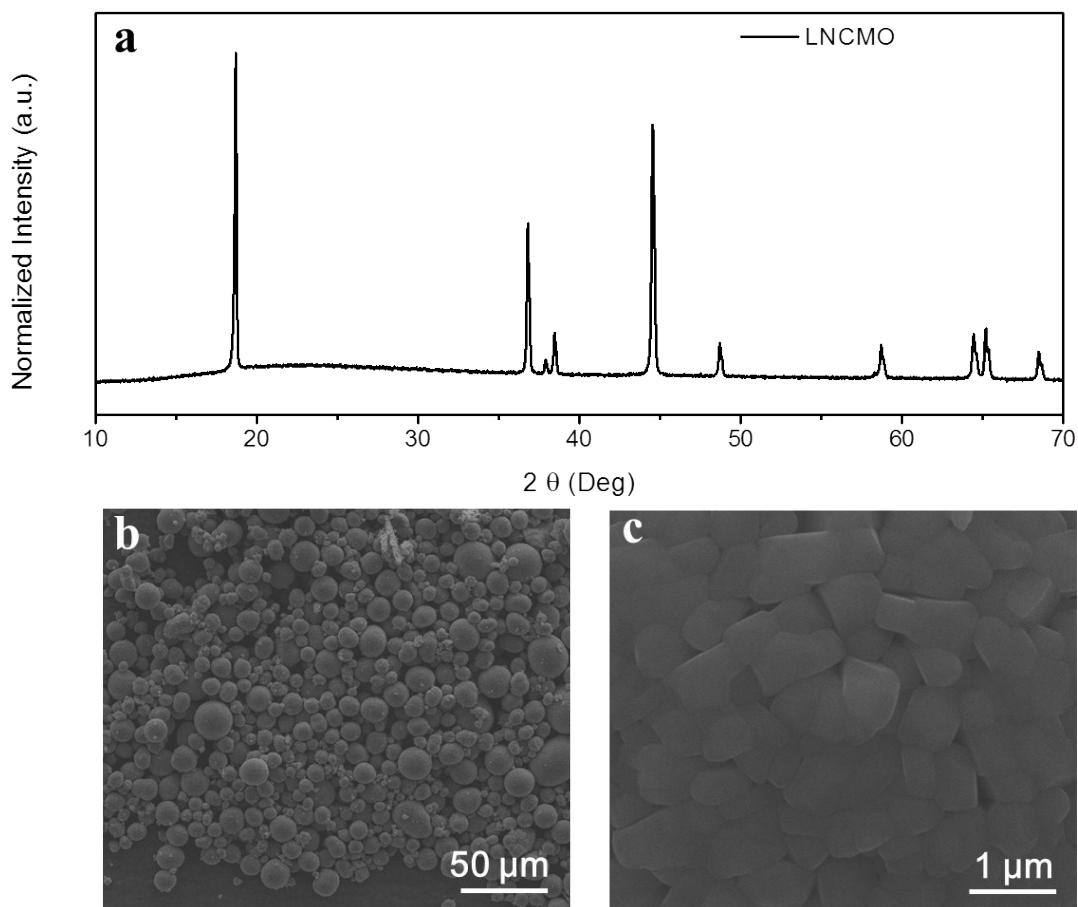


Figure S23. (a) SEM image and (b) magnified SEM image of CC@EC@LNCMO cathode. (c) XRD spectra of CC@EC@LNCMO cathode.

Commercial LiNiCoMnO_2 (LNCMO) was used as the cathode material due to their high voltage that could be beneficial in achieving high voltage lithium ion battery device. XRD pattern in Figure S23a confirm the LiNiCoMnO_2 phase of the cathode material. SEM images in Figure S23b shows the nanoballs morphology of the cathode. It can be seen from the enlarge SEM image in Figure S23c that the cube-like structure made up the nanoballs morphology.

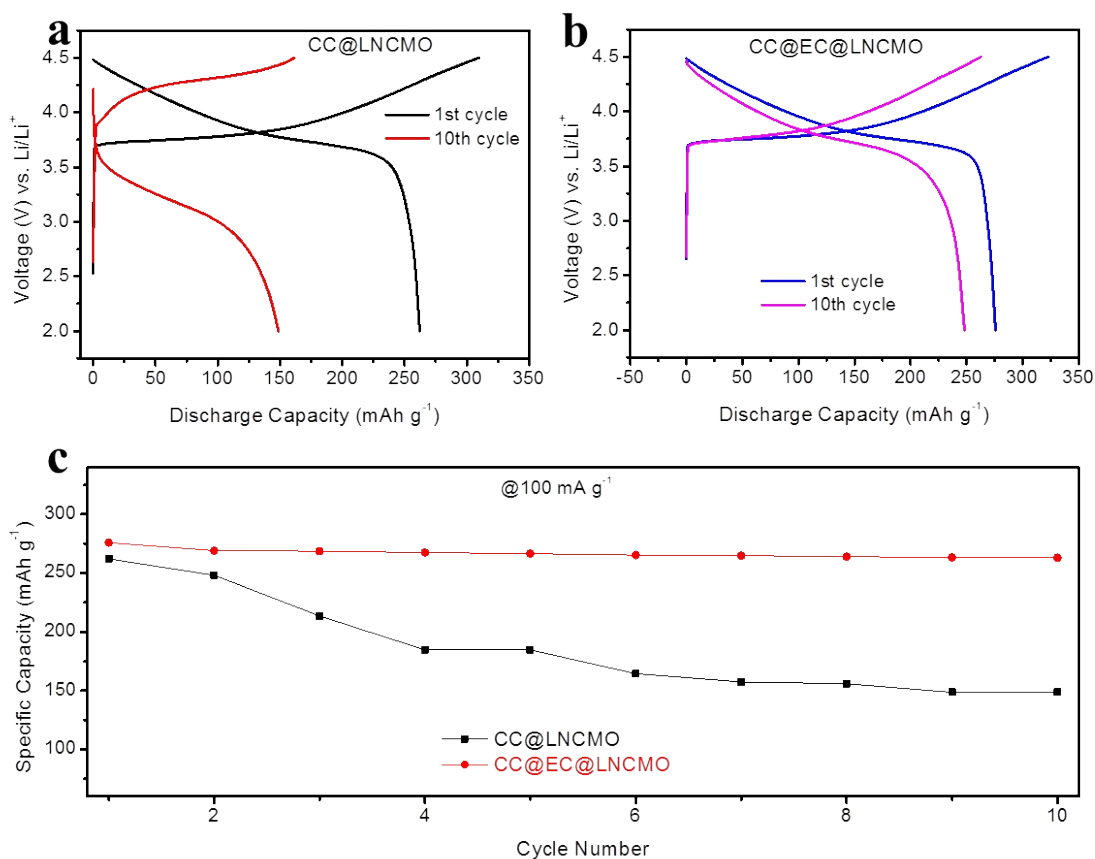


Figure S24. (a) 1st and 10th charge/discharge profile of CC@LNCMO. (b) 1st and 10th charge/discharge profile of CC@EC@LNCMO. (c) Cyclic performance of CC@LNCMO and CC@EC@LNCMO.

To study the electrochemical properties of the cathode, LNCMO was coated on CC and CC@EC to form CC@LNCMO and CC@EC@LNCMO electrodes, respectively. The 1st

discharge cycle of CC@LNCMO is 265 mAh g⁻¹ (Figure S24a), which is nearly the same with that of CC@EC@LNCMO at 275 mAh g⁻¹ (Figure S24b). CC@LNCMO electrode have loss much of its capacity retaining 55% of its initial capacity after 10 cycles (Figures S24c). However, CC@EC@LNCMO electrode retained 90% of its initial capacity after 10 cycles (Figures S24c). The excellent performance of CC@EC@LNCMO electrode is also attributed to CC@EC substrate that allows ions and electrons to be easily transported owing to the porous N-doped surface of CC@EC. Similar results have been reported in our previous work. ²

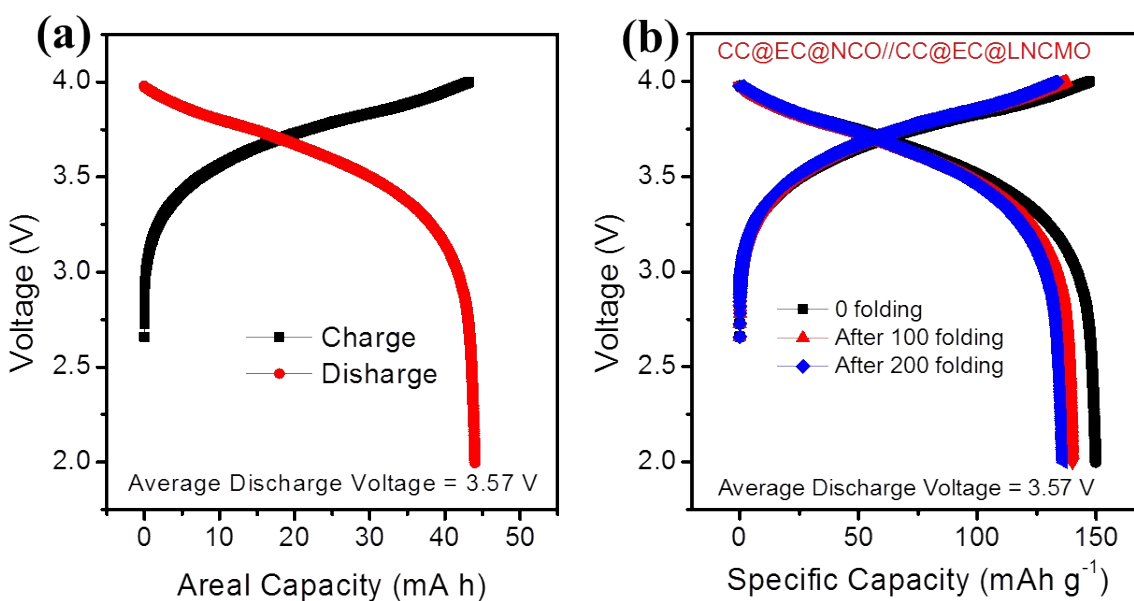


Figure S25. (a) 1st charge/discharge profile of CC@EC@NCO//CC@EC@LNCMO AFLIB based on mA h. (b) charge/discharge profile of CC@EC@NCO//CC@EC@LNCMO AFLIB after 0, 100 and 200 folding.

Table S1. A table showing the data in achieving the energy and power densities.

Discharge Capacity (mAh g ⁻¹)	Current Density (mA g ⁻¹)	Energy Density (Wh kg ⁻¹)	Power Density (W kg ⁻¹)
157	18	314	36
140	18	280	36
91.75	36	184	71
66.106	53	130	106
46.143	71	91	133
14.703	107	39	205

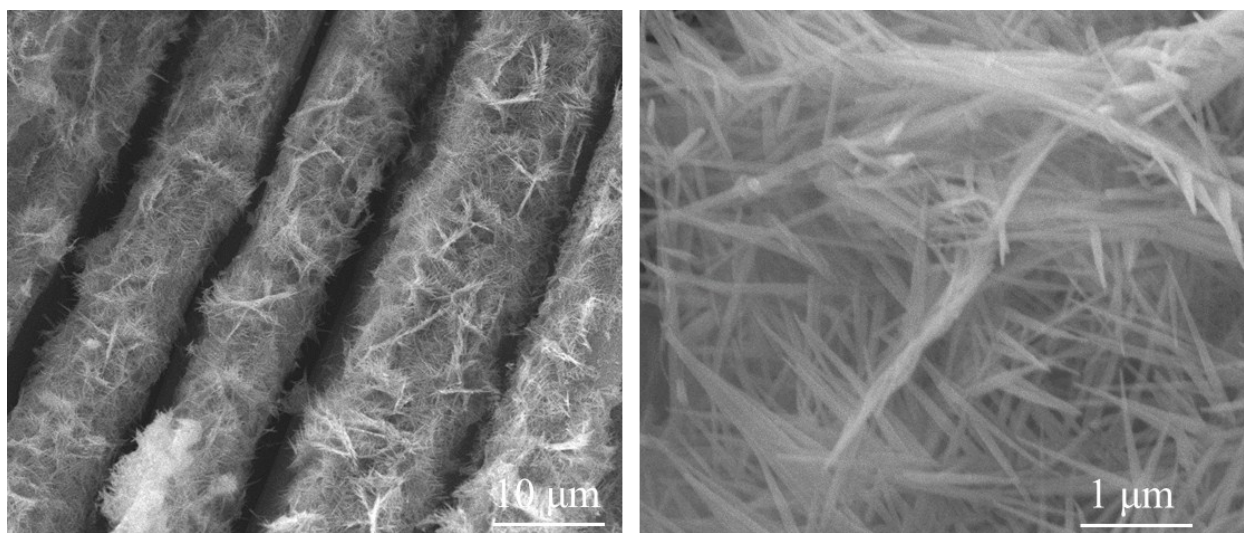


Figure S26. SEM images of CC@EC@NCO after 800 cycles.

References

1. M. J. Frisch, G. W. Trucks, H. B. Schlegel, G. E. Scuseria, M. A. Robb, J. R. Cheeseman, J. A. Montgomery, Jr., T. Vreven, K. N. Kudin, J. C. Burant, J. M. Millam, S. S. Iyengar, J. Tomasi, V. Barone, B. Mennucci, M. Cossi, G.; Rega, N. Scalmani, G. A. Petersson, H. Nakatsuji, M. Hada, M. Ehara, K. Toyota, R. Fukuda, J. Hasegawa, M. Ishida, T. Nakajima, Y. Honda, O. Kitao, H. Nakai, M. Klene, X. Li, , J. E. Knox H. P. Hratchian, J. B. Cross, C.

Adamo, J. Jaramillo, R. Gomperts, R. E. Stratmann, O. Yazyev, A. J. Austin, R. Cammi, C. Pomelli, J. W. Ochterski, P. Y. Ayala, K. Morokuma, G. A. Voth, P. Salvador, J. J. Dannenberg, V. G. Zakrzewski, S. Dapprich, A. D. Daniels, M. C. Strain, O. Farkas, D. K. Malick, A. D. Rabuck, K. Raghavachari, J. B. Foresman, J. V. Ortiz, Q. Cui, A. G. Baboul, S. Clifford, J. Cioslowski, B. B. Stefanov, G. Liu, A. Liashenko, P. Piskorz, I. Komaromi, R. L. Martin, D. J. Fox, T. Keith, M. A. Al-Laham, C. Y. Peng, A. Nanayakkara, M. Challacombe, P. M. W. Gill, B. Johnson, W. Chen, M. W. Wong, C. Gonzalez, J. A. Pople, Gaussian, Inc., Pittsburgh PA, 2009.

2. M.-S. Balogun, W. Qiu, F. Lyu, Y. Luo, H. Meng, J. Li, W. Mai, L. Mai and Y. Tong, *Nano Energy*, 2016, **26**, 446-455.